

# One Cell, One Drop, One Click: Hybrid Microfluidics for Mammalian Single Cell Isolation

Kenza Samlali, Fatemeh Ahmadi, Angela B. V. Quach, Guy Soffer, and Steve C. C. Shih\*

Generating a stable knockout cell line is a complex process that can take several months to complete. In this work, a microfluidic method that is capable of isolating single cells in droplets, selecting successful edited clones, and expansion of these isoclines is introduced. Using a hybrid microfluidics method, droplets in channels can be individually addressed using a co-planar electrode system. In the hybrid microfluidics device, it is shown that single cells can be trapped and subsequently encapsulate them on demand into pL-sized droplets. Furthermore, droplets containing single cells are either released, kept in the traps, or merged with other droplets by the application of an electric potential to the electrodes that is actuated through an in-house user interface. This high precision control is used to successfully sort and recover single isoclines to establish monoclonal cell lines, which is demonstrated with a heterozygous NCI-H1299 lung squamous cell population resulting from loss-of-function eGFP and RAF1 gene knockout transfections.

generate indels that differ between individual clones.<sup>[8–10]</sup> Isolating single clones provides a method for enriching correctly edited cells, of which one can correlate the phenotypic changes to a specific clonal genotype and facilitate downstream characterization.

The process of genome editing mammalian cells typically consists of in silico design of the guide, cloning the guide into an expression vector, transfection, selection, sorting, and expansion of homogeneous clonal lines.<sup>[11]</sup> Currently, the design of the guide and the act of transfecting cells can be done in less than a day.<sup>[11]</sup> Since new automation tools and methods are continuously being developed, the process of synthesis,<sup>[12]</sup> assembly,<sup>[13,14]</sup> and transfection<sup>[15–17]</sup> are becoming faster, cheaper, and more efficient. However,

selection and enrichment of transfected clones, especially in knockout experiments, sensitive cell lines, (e.g., human pluripotent stem cells h) or hard to transfect cell lines, remains a tedious and challenging task. Currently, common methods to isolate single clones are to use limited dilution or colony picking techniques to separate single isoclines and to generate a homozygous progeny.<sup>[18,19]</sup> The laborious and time-consuming process, the high dilution requirements, and the inherent probabilistic nature for limited dilution are not ideal for increasing the chances to obtain a single clone. Fluorescence-activated cell sorting (FACS), colony pickers, and other automated tools can provide a method to generate clonal cell populations, but are associated with high infrastructure and maintenance costs, the downstream optimization usually requires a large starting cell population, and their handling procedures can induce stress or an apoptotic response in the cells due to their high voltage requirements and physical handling.<sup>[20,21]</sup>

Droplet-based microfluidics systems are ideal for single-cell manipulation and analysis. These biocompatible systems mimic the physics of the cellular environment and in doing so, reduce the physical stresses often exerted on cells by traditional tools or robotic systems. They are also typically low in infrastructure and operational costs and operate under much lower volumes ( $\approx$ pL range).<sup>[22–25]</sup> Several researchers have already addressed multiple steps in the gene editing pipeline using microfluidics, including mammalian cell culture,<sup>[26,27]</sup> transfection of mammalian cells,<sup>[28–36]</sup> as well as the sorting or selection of transfected mammalian cells.<sup>[37]</sup> Droplet-in-channel microfluidics can operate in ultra high-throughput ranges while generating droplets containing a single cell.<sup>[38–41]</sup> A pitfall

## 1. Introduction

Gene editing in mammalian cells have become more accessible and less time consuming due to the availability of new editing tools that allow for rapid and precise edits. Using improved versions of CRISPR-Cas9,<sup>[1,2]</sup> and better methods to control the cell's double-strand break (DSB) repair mechanisms,<sup>[3]</sup> Cas9 has become a popular tool to engineer new cell lines. The utility of CRISPR is showing widespread benefits for generating new cellular therapies<sup>[4,5]</sup> and creating new genetic models for cancer.<sup>[6,7]</sup> To fabricate these new edited cell lines, evaluating the properties of single clones (i.e., a single edited cell) is especially important, as biallelic editing differences can occur and non-homologous end-joining DSB repair mechanisms

K. Samlali, F. Ahmadi, G. Soffer, Prof. S. C. C. Shih  
Department of Electrical and Computer Engineering  
Concordia University  
Montréal, Québec H3G 1M8, Canada  
E-mail: steve.shih@concordia.ca

K. Samlali, F. Ahmadi, A. B. V. Quach, G. Soffer, Prof. S. C. C. Shih  
Centre for Applied Synthetic Biology  
Concordia University  
Montréal, Québec H4B 1R6, Canada  
A. B. V. Quach, Prof. S. C. C. Shih  
Department of Biology  
Concordia University  
Montréal, Québec H4B 1R6, Canada

 The ORCID identification number(s) for the author(s) of this article can be found under <https://doi.org/10.1002/sml.202002400>.

DOI: 10.1002/sml.202002400

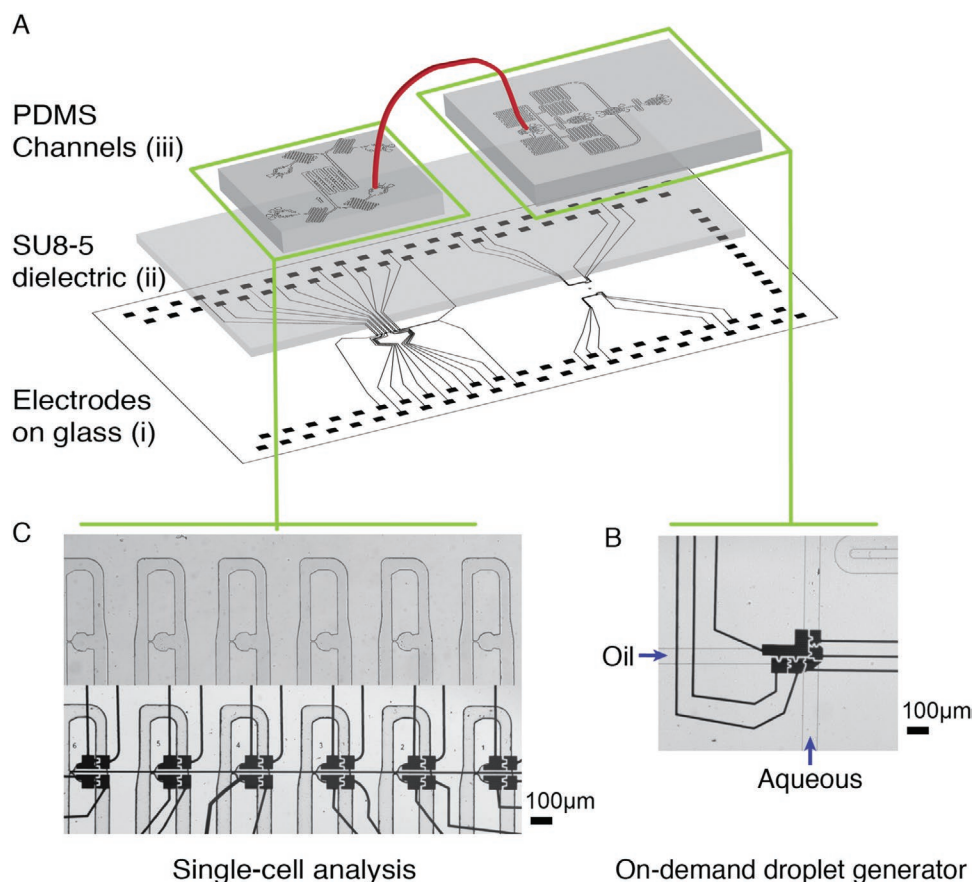


**Figure 1.** Integrated “hybrid” microfluidic device for on-demand single-cell encapsulation and analysis. The three layer device consists of a digital microfluidic layer with chromium electrodes patterned on glass, a 7  $\mu\text{m}$  thick SU-8 5 dielectric layer and a PDMS channel layer of channels of height 35  $\mu\text{m}$  and width of 50–75  $\mu\text{m}$ . B) The droplet generation device contains two T-junction droplet generators, under which several electrodes are located for on-demand droplet generation. C) The single-cell analysis device contains two inlets, and two outlets. The trapping area contains cell traps with 8  $\mu\text{m}$  constrictions, under which four electrodes are located. For details on channel, electrode and wiring sizes, see Supporting Information.

with these systems is that it is difficult to manipulate and to control the droplets in parallel. Digital microfluidics (DMF) can alleviate the challenges associated with droplet-in-channel systems since DMF are able to address each droplet individually. Having this control is especially useful in multi-step procedures, such as transformation and enzymatic assays,<sup>[42,43]</sup> drug and inhibitor screening,<sup>[44]</sup> and gene-editing<sup>[27]</sup> Recently, we have combined both of these platforms together, in which we call a “hybrid” microfluidics, placing co-planar electrodes (i.e., ground and activated electrodes on the same plate) under a network of microfluidic channels to enable individual control of the droplets in the channels.<sup>[45]</sup> Given the increased control over droplets and their contents,<sup>[46–51]</sup> there is an opportunity to use this hybrid-based technology as a method to control the isolation of mammalian isoclines.

Here, we have developed a deterministic “one-droplet-one-cell” hybrid microfluidics system that can trap single isoclines and subsequently encapsulate them in individual droplets. These single cell containing droplets can be released from traps in two directions, kept in position, or have the opportunity to be merged with other droplets, allowing this device to be used for various manipulations of the individual clones. To show the versatility of our device, we have shown its ability to establish

isoclonal mammalian loss-of-function cell lines from gene knockout experiments by sorting and recovering engineered clones of a NCI-H1299 lung squamous cell carcinoma.

## 2. Results and Discussion

### 2.1. The Design of a Hybrid Microfluidics System for Single-Cell Manipulations

**Figure 1** depicts the representative device used for single-cell trapping, single-cell droplet generation and a variety of droplet operations. As shown in Figure 1A, the microfluidic device consists of three layers: a patterned electrode layer, a 7  $\mu\text{m}$  SU-8 5 dielectric layer and a PDMS-based channel layer of 35  $\mu\text{m}$  height and a main channel width of 50  $\mu\text{m}$ . The “hybrid” signifies integrating droplet and digital microfluidics onto a single device—consisting of a bottom digital microfluidic layer (i.e., metal electrodes and dielectric) along with a top patterned channel layer in which cells are trapped (single-phase) or aqueous droplets are manipulated in an oil phase (two-phase).<sup>[45]</sup> The device is divided into two sections: 1) an on-demand T-junction droplet generator and 2) an array of trapped droplets containing single

cells. As shown in Figure 1B, the on-demand droplet generation consists of co-planar electrodes that will actuate the aqueous flow (using electric potentials) to the orthogonal continuous oil flow that will break the continuous aqueous flow into discretized droplets. The single-cell droplet array (Figure 1C) can trap single cells, after which they are encapsulated in droplets that are generated within the traps by the application of an electric field. It contains 12 traps, of which six, are equipped with electrodes. Tubing bridges the two parts of the device to transfer the droplets from the droplet generator to the single cell analysis part of the device. The device contains two inlets—I1 for oil and droplets and I2 for cells and priming—and two outlets—O1 for waste and O2 for sample recovery and flow reversal—(Figure S1, Supporting Information).

In designing the system shown in Figure 1, there is a design element that requires consideration for reliable cell trapping and encapsulation. Two commonly used methods for single cell isolation—trapping and encapsulation—are complementary. The traps are designed such that they could trap single cells with high efficiency, yet also allow for a smooth phase change to a two-phase flow. We have followed resistance based design guidelines as reported for microfluidic serpentine trap designs used for trapping droplets and cells.<sup>[52–57]</sup> The design element concerns the location of the traps relative to the main channel such that both single-cell trapping, and a phase change can occur. By modeling the flow rate profile and the velocity streamlines, we optimized the channel geometry (Figure S2, Supporting Information), such that volumetric flow rate through the trap ( $Q_{\text{trap}}$ ) is greater than volumetric flow rate through the bypass channel ( $Q_{\text{bypass}}$ ) when there is no cell in the trap. We found that positioning the trap near the curvature of the main channel (i.e., the end of a serpentine channel) along with a narrow ( $\approx 50 \mu\text{m}$ ) trap entrance and a narrow ( $\approx 50 \mu\text{m}$ ) main channel width immediately after the trap opening, prevented cells bypassing the empty traps. The optimized placement offers a higher effective hydrodynamic resistance in the bypass channel ( $R_{\text{bypass}}$ ) than through the trap ( $R_{\text{trap}}$ ). Hence, the flow rate in the trap is higher compared to the bypass channel ( $Q_{\text{trap}} > Q_{\text{bypass}}$ ) to maintain the same pressure drop (as shown from other studies<sup>[58]</sup>). Furthermore, the design offers two additional advantages: 1) if a cell is trapped, it is unlikely for another cell to flow into the same trap since this increases the  $R_{\text{trap}}$  (and reduces  $Q_{\text{trap}}$ ) and 2) during a phase change for single-cell encapsulation (in situ droplet generation as described below), the resistance in the trap is sufficiently higher than the bypass channel which will help preventing squeezing the cells out of their traps. A mathematical description and the simulation details are described in Notes S1 and S2, Supporting Information.

Finally, we also note that one of the main goals of this work is to automate the process of actuation and droplet manipulation, but a key challenge is to integrate and to control the multiple pieces of hardware into one software framework. In this work, the microfluidic device is connected to two main hardware components: the in-house automation system (i.e., optocoupler switches) and a syringe pump system (Figure S3, Supporting Information). The automation system serves the purpose to provide electrode actuation and the syringe pump system is to control the flow rates in the device.<sup>[43,59]</sup> Since these

two hardware systems are operating on different software protocols, we developed our own Python based framework with a simple user interface. The system user can control the flow of certain fluids (start, stop, flow rate), and perform several pre-programmed droplet manipulations via click-of-a-button (e.g., “encapsulate”, “forward release”, “reverse release”, and “keep” for a specific actuation time). The software is open-source and available to download at <http://bitbucket.org/shihmicrolab>.

## 2.2. Hydrodynamic Single-Cell Trapping and Deterministic Single-Cell Encapsulation through In Situ Droplet Generation

Figure 2 illustrates the optimized device operation procedures for trapping single cells and encapsulating the cells inside droplets using a “hybrid”-based microfluidics platform. As detailed in the Experimental Section, the device operation procedure consisted of priming, cell loading, phase change, and encapsulation followed by droplet release (see Note S3, Supporting Information for automation control). This workflow, and the procedure for trapping, and in situ encapsulation are represented as a schematic (Figure 2) and as a video (Video S1, Supporting Information). First, devices were primed with 2% Pluronic F-127 for at least 5 min to decrease cell adhesion to the PDMS. Second, an aqueous flow containing fresh media with mammalian cells (MCF-7 breast cancer cell line) was introduced into the trapping device at a concentration of  $10^5$ – $10^6$  cells  $\text{mL}^{-1}$  (see Figure 3A for an image of six individually trapped cells). We have evaluated the efficiency of cell trapping as a function of flow rate. Using our design, the optimal range of flow rates to trap individual cells is between  $1$ – $4 \text{ nL s}^{-1}$  (Figure 3B). At this range of flow rates, cells are unlikely to occupy traps with multiple cells and the MCF-7 cells do not squeeze through the traps (unlike at high flow rates; see Video 2, Supporting Information). Single cells are efficiently trapped ( $\approx 88.3\%$ ) at  $5 \text{ nL s}^{-1}$ —an efficiency similar to previous studies which required displacement structures or other external forces to trap cells.<sup>[60–62]</sup> We counted over 54 consecutive events (out of 54 observations) of MCF-7 cells passing by a single MCF-7 cell occupied trap without trapping a second one. The conditions for success at these flowrates are 1) the optimized channel flow velocity profile and the slanted overhang along the main channel (close to the trapping region) to steer the flow towards the trap, 2) the design of a  $8 \mu\text{m}$  constriction which is smaller than the cell size, and 3) the physical properties of MCF-7 cells (i.e., lower deformability).<sup>[52,58]</sup>

Following the trapping of the cells is the generation of a droplet within a trap which results in the encapsulation of a single cell inside a droplet. Popular passive single-cell encapsulation is known to be a procedure that follows Poisson statistics, generating droplets with none, one or more cells.<sup>[63]</sup> Using the hybrid device, we can generate a droplet in situ, and thus deterministically encapsulate the trapped cell. This is done by moving from a single-phase flow to a two-phase flow using a phase change procedure by: 1) flowing an oil phase through the entire channel and 2) applying an electric potential to the electrodes below the trap when the oil flow approaches. Figure 3C shows three images taken from video frames depicting the on-demand, in situ droplet generation process. Four coplanar

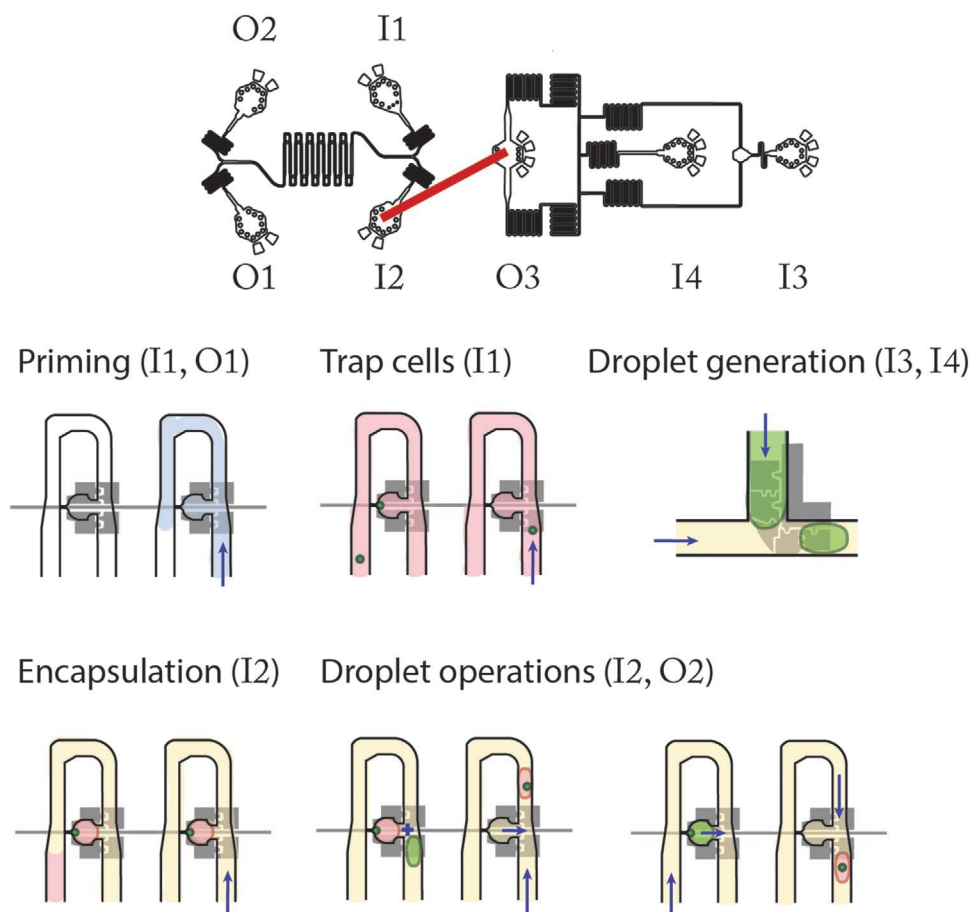


**Figure 2.** Workflow of device operation. Priming the device with 2% Pluronic F-127 in PBS for 5 min. MCF-7 cells in PBS are trapped. On-demand droplet generation can be selected to generate droplets, after which the aqueous flow is stopped. When all traps are loaded, oil (HFE 7500 2% Ran Fluorosurfactant) is loaded at  $4 \text{ nL s}^{-1}$  by connecting the droplet bridge. Oil flow shears off a small volume of remaining PBS, which forms a droplet around the cells. Droplets are flowed through the droplet bridge and various droplet operations (trap, release, keep, merge) can be performed. Oil flow can be reversed to collect droplets. The inlet (I#) and outlets (O#) represents where the tubing is inserted for each operation.

electrodes (size  $\approx 100 \mu\text{m}$ , area  $0.06 \text{ mm}^2$ ) are used for the generation event—two electrodes below the main channel and two electrodes below the trap. In Frame I, an electrode below the trap is activated. An oil flow enters the main channel for the purpose of a phase change. In Frame II, the electrode below the trap is activated while the other electrodes are grounded. The aqueous phase and the single-cell remain inside the trap when the oil flow (in the main channel) “cuts” the aqueous phase at both ends of the trap. Generated cell containing droplets are on average  $150.3 \pm 5.6 \text{ pL}$  in volume ( $N = 11$ ). In Frame III, all potentials are grounded, and the oil phase flow continues to the next trap to perform the next encapsulation procedure. To aid the design of the trap and to determine the optimal actuation sequence, we have simulated the electric potential and electric field distributions (Figures S4 and S5, Supporting Information). As shown, the electric field density ( $\approx 5 \times 10^6 \text{ V m}^{-1}$ ) is induced between the main channel and the trapping region. This field gradient induces an electrostatic force that will pull the liquid towards the trap (similar to droplet actuation on a DMF device<sup>[64]</sup>). Given this capability, the device encapsulate cells in droplets on-demand without Poisson-based statistics. The details of the simulation are described in Note S2 and

Table S1, Supporting Information. To our knowledge, this is the first occurrence of in situ droplet generation for deterministic single-cell encapsulation, providing an alternative to Poisson based encapsulation methods.

The success of trapping and encapsulation is highly dependent on device fabrication and operation methods. For example, the reliability of electrode actuations and resulting droplet operations heavily depends on the alignment of the electrodes and channels. To minimize the strenuous task of alignment, we used the ground wire and the gap between electrodes to serve as an alignment mark. Since these are clear marks, alignment can be performed swiftly under a microscope without losing the oxygen plasma treatment on the PDMS.<sup>[65]</sup> Furthermore, we divided the device into two components (droplet generator and serpentine trapping channel) to fit the features within the field-of-view the microscope, and to minimize PDMS shrinkage.<sup>[66]</sup> The process of inserting and removing tubing from the inlets and outlets also require slow manipulation. The air bubbles are most likely to occur when changing from priming solution to cell solution and when initiating the oil flow. This is because the bubbles can block flow inside traps and push cells out of their traps, which will also

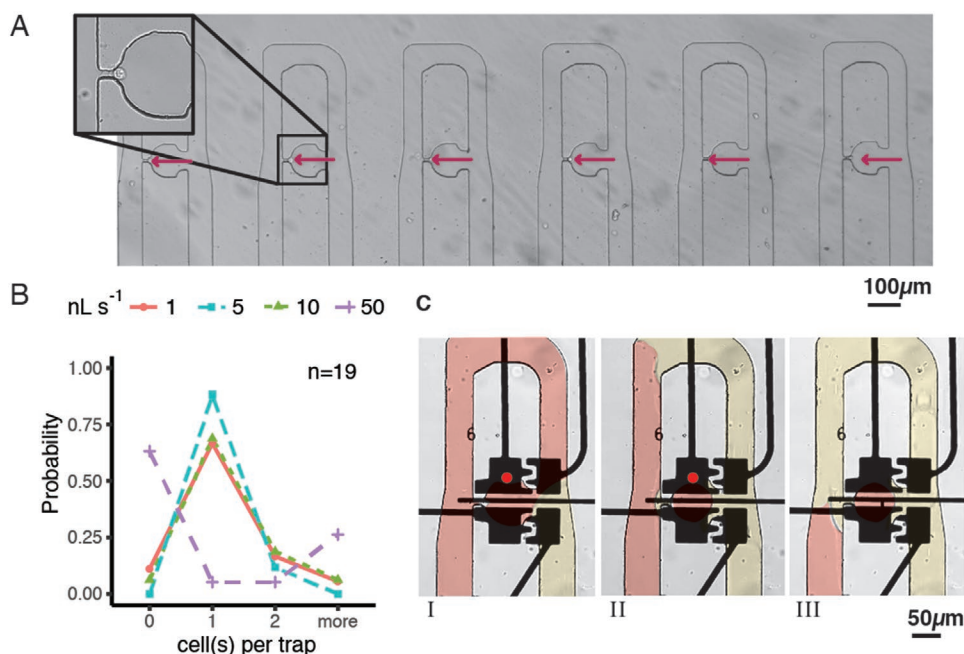


**Figure 3.** Cell trapping and encapsulation A) Single MCF-7 cells are trapped in PBS (bright-field, 4X). B) Efficiency of trapping cells at different flow rates. The cell concentration was kept constant at  $5 \times 10^5$  cells mL<sup>-1</sup> in PBS. C) Encapsulation procedure. Frame I: A single MCF-7 cell is trapped. An HFE 7500 + 2% Ran surfactant is loaded into the device at 4 nL s<sup>-1</sup>. The trap electrode is actuated (15 kHz, 126 V<sub>RMS</sub>). Frame II: A droplet is formed within the trap and the oil phase continues through the bypass channel. Frame III: An encapsulated MCF-7 cell.

disturb the stability of the fluid flow causing erratic flow rates. The air bubbles can also cause unwanted pressure differences inside the channel, which may lead to droplet breakup and movement. Our solution is to insert the tubing gently at high flow rates and use a small diameter tubing to bridge the droplet generator and the trapping device (more info in Note S4, Supporting Information). Lastly, it is important to perform a thorough cleaning of the traps by removing the remaining oil emulsions in the 8 μm trap constrictions to ensure high cell trapping efficiency for the next set of trapping experiments.

### 2.3. Two-Phase On-Demand Droplet Operations: Droplet Generation, Releasing and Keeping of Droplets in Traps

After trapping and phase change, we turned our attention to other droplet operations such as droplet generation and keeping or releasing the droplets containing single cells (Video S3, Supporting Information). Generally, in droplet-based microfluidics, controlling droplet positions inside the channels is performed by using passive structures,<sup>[52,55,58]</sup> valves,<sup>[67,68]</sup> or external forces (optical, acoustic, dielectrophoresis).<sup>[55,69,70]</sup> For example, Sauzade et al.<sup>[52]</sup> uses serpentine channels containing droplet traps under forward flow to trap droplets and uses reverse flow to hydrodynamically release droplets. The platform presented here can perform multiple droplet operations, such as “trap” operation under forward flow, “release” operation under forward/reverse flow, and “keep” operation under reverse flow. Our device has no additional channel structures that have been fabricated to direct the cells in flow and there is no reliance on synchronizing the droplet flow to control the droplets

as required by previous works.<sup>[71,72]</sup> The main contributor to controlling the droplets on our device is the application of electric potentials to the electrodes (similar to digital microfluidic systems<sup>[73]</sup>) such that the above-mentioned operations can be performed with high fidelity.

To characterize releasing operations, we have tested the likelihood for droplet release at different flow rates (for the forward and reverse flow directions) using electric potential or via pressure-driven flow. **Figure 4A** (Frames I–IV) shows the actuation sequence for releasing a droplet under forward flow. The droplet is released by actuating electrodes below the trap (Frame II) followed by activating an electrode below the main channel and the trap (Frame III). By using this specific sequence, the electric field density directs the droplet from the trap towards the main channel in the direction of the flow (Figure S5, Supporting Information). We also tested the likelihood for droplet release at different flow rates in forward direction (from inlets to outlets) (Figure 4B). As shown, low forward flow rates (<1 nL s<sup>-1</sup>) give rise to higher probability (>95%) of being able to release the droplet. Since droplets are trapped due to the hydrodynamic pressure,  $P_h$ , the oil flow and the droplet are controlled by using electrostatic forces ( $F_{elec}$ ). Droplets are released when the electrostatic force  $F_{elec}$  is greater than the  $P_h$  generated by the flow in the main channel. This relationship also holds true when there is no flow rate applied. In this case, the droplet is released from the trap but is static at the entrance of the trap since there is no flow. While without any electrostatic force (i.e., no electric field applied) at any given flow rate, the droplet is never released from the trap.

Next, we tested the likelihood of releasing droplets with reverse oil flow, with and without on-demand actuation. As

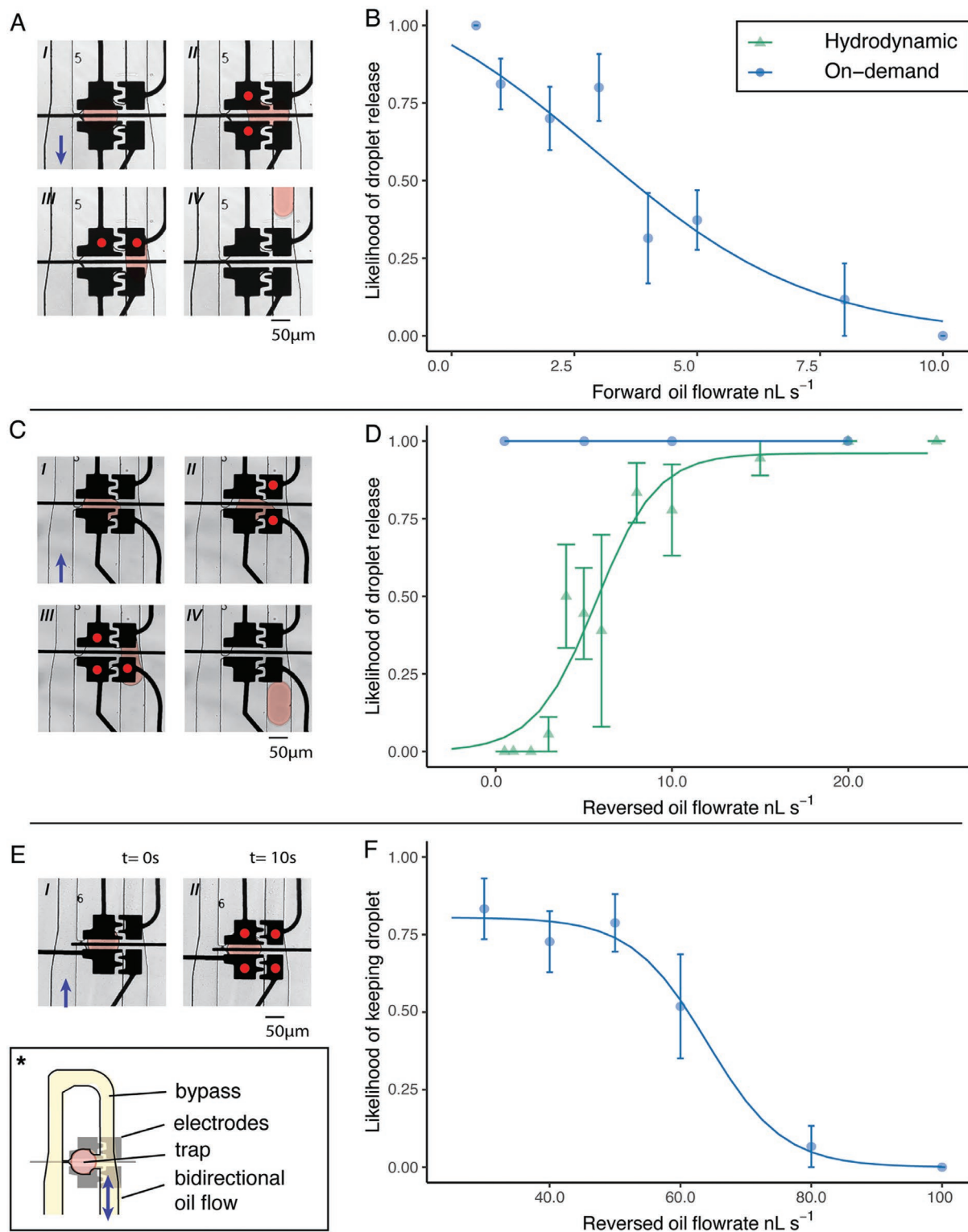


**Figure 4.** On-demand droplet operations. Actuation patterns are indicated with a red dot (bright field, 15×). Bypass channel, trap and flow are as indicated (\*). The droplet is falsely coloured for clarity. A) Actuation sequence of releasing a droplet towards an outlet using on-demand functionality (15 kHz, 126 V<sub>RMS</sub>). B) Efficiency of release of droplets under forward flow rates. (*n* = 8, 10 replicates per trap) C) Actuation sequence of releasing droplet towards the inlets using on-demand functionality. (15 kHz, 126 V<sub>RMS</sub>) D) Efficiency of release of droplets under reversed flow rate. Hydrodynamically, droplets are released more efficiently towards the inlet with increasing flow rates. With on-demand release, droplet show perfect release regardless of flow rates tested. E) Actuation sequence of keeping droplets within the trap under reversed flow rate. (15 kHz, 126 V<sub>RMS</sub>, 10 s) F) Efficiency of keeping droplets on-demand under reverse flow rate. Droplets can be kept efficiently for flow rates lower than 45.4 nL s<sup>-1</sup>.

shown in Figure 4C (Frames I–IV), the actuation sequence under reverse flow (from outlets to inlets) is similar to the actuation sequence for the droplet release under forward flow. In contrast to with forward flow, the probability of releasing a droplet is most likely to occur at higher flow rates ( $>10.92 \text{ nL s}^{-1}$ ) (without actuation; hydrodynamic flow only). The lower flow rates are more likely to keep the droplet inside the trap (Figure 4D)—a similar trend observed in another study.<sup>[74]</sup> When actuation is implemented, the droplet can be released from the trap at any given time and there is no dependence on the reverse flow rate using a specific actuation pattern. This is an exciting result since it enables the user to release and to select droplets on-demand without the need for dielectrophoretic, acoustic or magnetic sorting techniques. Thus, this represents a significant advance over other droplet-based microfluidic systems that implement trapping and releasing droplets.

In some cases keeping droplets inside a trap is also a desired operation.<sup>[45,75,76]</sup> Figure 4E shows the actuation sequence for keeping a droplet. Four electrodes are activated to ensure the highest electric field density, which is centered at the opening of the trap to prevent the droplet from escaping into the main channel (Figure S5, Supporting Information). The likelihood of the droplet being released when different flow rates are applied from the narrow to the wider region of the trap shows flow rates below  $45.4 \text{ nL s}^{-1}$  give rise to higher probability on keeping the droplet ( $>95\%$  logistic regression model asymptote) ( $N = 10$ ) (Figure 4F). The main reason for this trend is that after a certain flow rate,  $P_h > F_{\text{elec}}$ . However, if the flow rate decreases, droplets reside for a longer period within the main channel, which can be disadvantageous for fast sorting procedures (Figure S6, Supporting Information). It is possible to increase the applied potential ( $>126 \text{ V}_{\text{RMS}}$ ) to the electrodes (to increase the electrostatic force and work under higher flow rates), but this may induce dielectric breakdown,<sup>[77–79]</sup> followed by electrolysis or Joule heating which can ultimately lead to cell stress and to changes in genomic regulation in cells.<sup>[80]</sup> Hence, for gene-editing experiments discussed below, we used flow rates below  $45 \text{ nL s}^{-1}$  to keep the droplets inside the trap while maintaining applied potentials below  $126 \text{ V}_{\text{RMS}}$ .

Similar to our previous work, we generate droplets on-demand to have the capability to add reagents to other droplets in the device.<sup>[45]</sup> Ahmadi et al.<sup>[45]</sup> recently reported the first hybrid microfluidics device that is capable of generating droplets on-demand by combining the pressure of the continuous oil phase and the electrostatic actuation of the aqueous flow. The desire to have control over droplet generation is an important step forward for the field, as the enthusiasm for droplet control in droplet microfluidic devices is well-documented.<sup>[81]</sup> We improved upon this work by designing an automated replenishment of the aqueous flow, which removes the limit on the number of droplets that can be generated. Using this droplet generator, we are able to generate droplets on-demand using a T-junction configuration with oil flow rates between 2 and  $2.5 \text{ nL s}^{-1}$  (Figure S7, Supporting Information). From our observation, lower flow rates than  $2.0 \text{ nL s}^{-1}$ , on-demand droplet generation became difficult due to the inability of the oil flow to shear off a droplet, while at higher flow rates greater than  $2.5 \text{ nL s}^{-1}$  the pressure of the oil flow is larger than the electrostatic force removing the force balance at the interface to

generate droplets. After droplet generation, we have shown the capacity of the device to merge droplets. As shown in Figure S8, Supporting Information, we can merge incoming droplets with trapped droplets on demand. An advantage of on-demand merging is that it does not rely on the tedious synchronization of two streams of droplets for droplet coalescence nor does it require any pressurized channel.<sup>[46,72,82–87]</sup> Generating droplets on-demand with a T-junction and generating single-cell containing droplets by phase change, show high monodispersity ( $250.9 \pm 39 \text{ pL}$  and  $150.3 \pm 55.6 \text{ pL}$  respectively) (Figure S7 and Table S2, Supporting Information). The compendium of results in Figure 4 represent important additions of multiple on-demand droplet manipulations with individual and parallel droplet control for droplet-based microfluidic systems. These droplet operations, in addition to the deterministic encapsulation, provide a powerful device for sorting and selecting individual isoclines (as described below).

Droplet-based microfluidic platforms typically use short pulses of electric potentials to either sort droplets<sup>[88]</sup> or manipulate droplets on an array of electrodes.<sup>[27]</sup> In these platforms, a droplet containing a biological cell experience a negligible electrical field and therefore their viability is maintained.<sup>[80,89]</sup> We further investigated the effects of electrode actuation on cells in single-phase fluid, before cells were encapsulated. This is representative of electrode actuation for single-cell encapsulation. After priming the device and trapping the single MCF-7 cells, we performed a viability assay by flowing a solution of fluorescein diacetate ( $\lambda_{\text{ex}}$ : 490 nm,  $\lambda_{\text{em}}$ : 526 nm) and propidium iodide ( $\lambda_{\text{ex}}$ : 488 nm,  $\lambda_{\text{em}}$ : 617 nm) through the channel labeling live and dead cells respectively. We compared the viability of voltage-potentiated and non-potentiated cells immediately after 30 s application of a low frequency AC electric potential. As Figure 5A illustrates, the single cells are generally viable (shown in green) after being exposed to electric fields on the hybrid device compared to non-exposed cells. There was no significant difference between the cells directly exposed to the potentials and non-potentiated cells (Figure 5B;  $P = 0.6687$ ). We do observe a small loss of viability ( $\approx 18\%$ ) in the potentiated cells and observe a similar viability ( $87.5 \pm 7.2\%$ ) in the non-potentiated cells. We believe the reduction in viability is attributed to the pre-processing sample handling procedures outside their native cell culture environment, for example, cell sample preparation in the syringe. Regardless of the reasons for the loss, these initial results for viability suggests that actuating electrodes in our hybrid device does not significantly alter the cell viability ( $>80\%$ ) and is suitable for our isoclonal procedures (described below).

#### 2.4. Recovery and Expansion of Single-Cell Isoclines from a Heterogeneous Engineered Cell Population

To illustrate that our hybrid platform is suitable for single cell isoclonal sorting, we followed a gene-editing workflow to isolate the engineered cell from a heterogeneous cell population of an NCI-H1299 lung squamous cell carcinoma cell line.<sup>[90,91]</sup> As shown in Figure 6A, two plasmids containing Cas9 and a sgRNA, targeting either the eGFP or the RAF1 gene were used for transient lipid based transfection. We evaluated the transfection efficiency

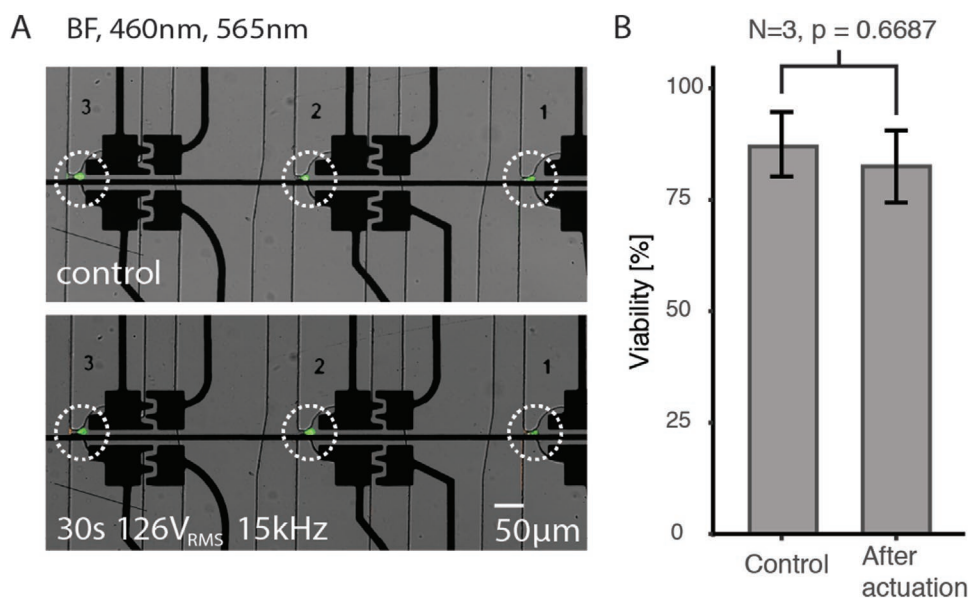


**Figure 5.** Viability assay of MCF-7 cells. A) Trapped MCF-7 cells stained with FDA/PI after 10 min incubation on device (top), and after total actuation time of electrodes of 30 s (15 kHz, 126 V<sub>RMS</sub>) and 10 min incubation on device (bottom). FDA stain reveals live cells and PI stain reveals dead cells. B) A cell viability plot shows no significant difference in viability between the control (87.5 ± 7.2%) and after actuation of electrodes (82.5 ± 8.1%) (unpaired two-sample *t*-test, *p* = 0.6687, *N* = 3).

for each knockout experiment and observed a ≈25.3% and a ≈13.7% efficiency for eGFP and RAF1 respectively (Figure 6B; Figure S9, Supporting Information). Knockout efficiencies were determined by a genomic cleavage detection assay and were calculated to be 4.95% and 8.3% for eGFP and RAF1 respectively (Figure 6C). Since we obtained a heterozygous population (Figure S10, Supporting Information), this called for a precise mechanism to sort and to isolate the low population of successful clones. Hence, for this part of the workflow, we used our hybrid device by trapping the cells in the device such that they can be imaged by fluorescence microscopy to determine which cells have been transfected (mCherry expression) (Figure 6D; Figure S11, Supporting Information). Given the low number of successful clones, we predict that only one out of six traps are to contain a successful transfected cell (≈16.7%) (Figure 6E). Indeed, there are times when the traps did not fill with a transfected clone, however, with fine-tuned control and automation, our system can increase the flow rate in the forward direction which enabled the cells to squeeze through the traps such that a new cell can be trapped. This is one of the key capabilities of this device—trapping and releasing of isoclonal cells can be performed iteratively. In merely 45 min (instead of hours), isoclonal cells can be trapped, encapsulated and sorted since 1) there is no requirement for iterative sample preparation or 2) isolation of a clonal cell line by limited dilution or other time-consuming techniques such as FACS is no longer needed.<sup>[11]</sup> After encapsulation of a successful isoclonal (Video S4, Supporting Information), on-demand forward release of a single-isoclonal in a droplet was performed to recover the isoclonal (Figure 6F).

Expansion is a key step for the development of a new clonal cell line. After droplet sorting in microfluidic devices, the droplets can be recovered by directly flowing them into a different substrate for the recovery of cells using a chemical emulsion breaking method,<sup>[92]</sup> centrifugal methods,<sup>[93,94]</sup> or automated

dispensing methods.<sup>[95,96]</sup> As these methods are performed on emulsion of multiple droplets, we were unsuccessful at using these techniques to recover only the content of a single drop. The deterministic encapsulation and on-demand release of droplets in our platform allowed us to develop a method to recover the content of a single droplet from a water-in-oil emulsion into a single well of a 96-well plate (see Figure S12, Supporting Information). Following an on-demand forward release of a single isoclonal, we used a method similar to Langer et al.<sup>[97]</sup> by transferring the droplet into a capillary and onto a hydrophobic PTFE membrane (Figure S12, Supporting Information). The oleophilic membrane absorbs the HFE 7500 oil, removing the surrounding oil around the aqueous droplet. We washed the emulsions with FC-40 oil to remove excess HFE and surfactants and to release the isoclonal into a media droplet which is subsequently transferred to a 96-well plate. As shown in Figure 6F are images of the eGFP knockout isoclonal cells being expanded in a 96 well plate format on day 5 and day 7. The mCherry reporter is not used after day 3 since the plasmid is transiently transfected and therefore is lost after several cell divisions (i.e., after 2–3 days post-transfection).

The results described above demonstrate that hybrid-based microfluidics can be used to expedite the gene-editing workflow with very high performance and efficiency. With efficient trapping, encapsulation, releasing, recovery, and expansion procedures, hybrid microfluidic devices outperform the standard FACS and limited dilution assays for isolating single clones. These data presented here gives researchers interested in gene-editing the ability to establish monoclonal lines from heterozygous transfected populations, without the excessive manual handling steps required for selection, sorting, dilution, and clonal selection. In continuing work, we are using these devices (or derivative thereof) for low-transfection cell lines, which should highlight the advantages further by application to engineering cellular-based therapies.

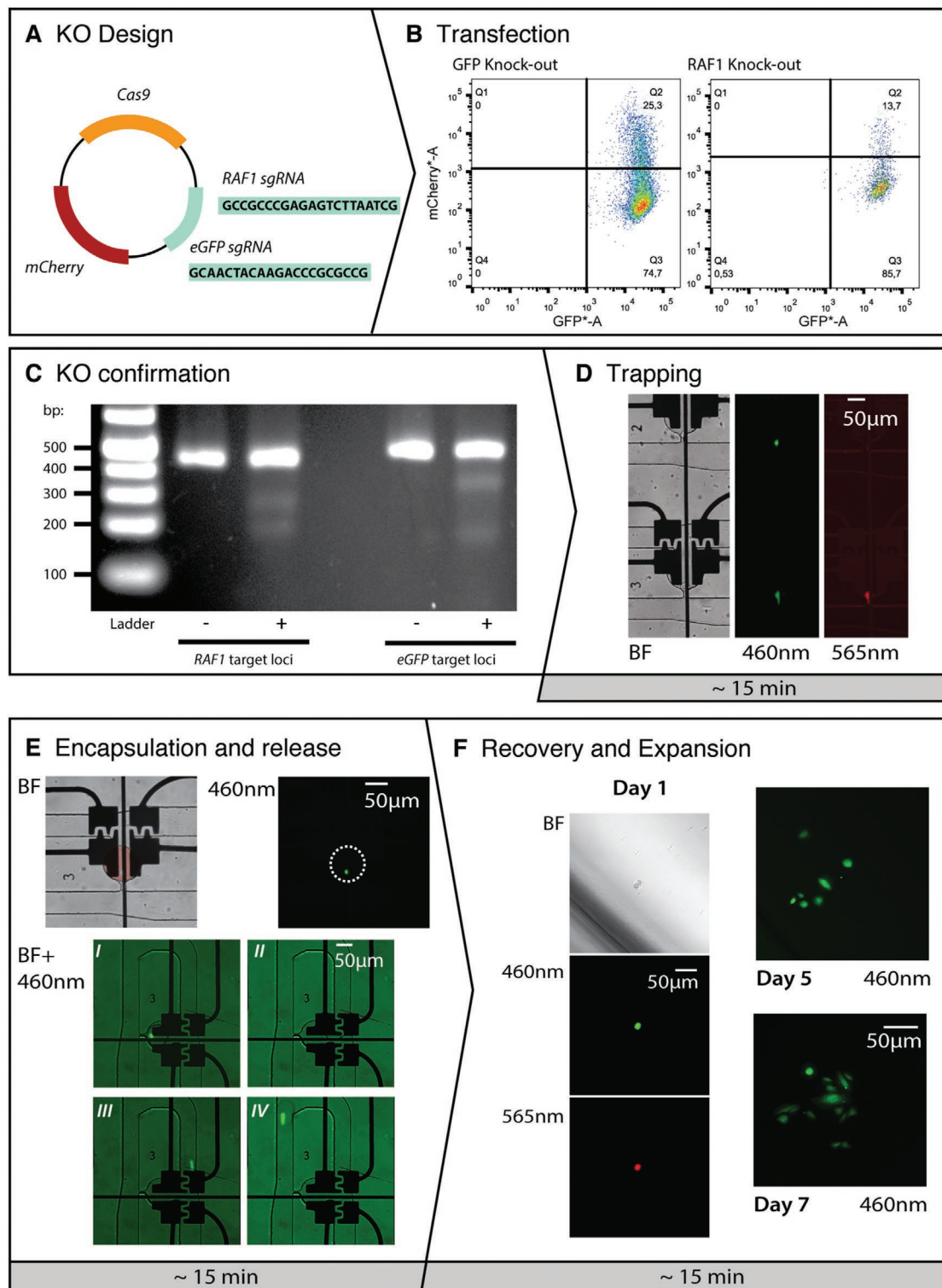


**Figure 6.** Gene-editing pipeline: screening and sorting edited H1299 isoclones. A) Design of a plasmid containing the Cas9 gene, a mCherry reporter, and sgRNA targeting either eGFP or RAF1. B) Flow cytometry indicating transfection efficiencies. C) Knockout confirmation through a genomic cleavage detection assay. D) H1299 cells (eGFP+) resulting from lipid mediated transfection were trapped and screened for mCherry expression (red). Trapped cells show successful transfected cells expressing both mCherry (red) and GFP (green) (trap 3) and a cell only expressing native GFP (green) (trap 2). E) The transfected isoclone was encapsulated and subsequently released on-demand towards the outlets (trap 3, Frames I–IV from a video show the release of a single clone in a droplet). F) The droplet containing the isoclone knocked out cell is collected from the outlet, transferred into a capillary, and recovered into a 96-well plate. Two images showing expansion of the knocked out GFP isoclone cell on day 5 and day 7. The mCherry reporter gene is only shown on day 1 since it is lost through cell division after day 2 or 3.

### 3. Conclusion

The combination of hydrodynamic pressure and electrostatic force offered in a three-layer hybrid microfluidic device, was used to control flow in a cell and droplet trapping channel. First, we showed that reliable single-cell trapping can be followed with a deterministic encapsulation of the trapped single-cells. Using a phase change and electrode actuations, the one-phase cell containing aqueous flow can be turned into a droplet based two-phase flow. Next, we showed efficient droplet controllability and fully characterized the efficiency of droplet generation, bi-directional release and keeping. All of these operations, including deterministic encapsulation, can be performed with a “click of a button” automation approach.

We applied this system to sort and to recover gene-edited single cells from a NCI-H1299 non-small cell lung carcinoma cell population. Single cells from the heterozygous knockout population were encapsulated and sorted based on expression of a reporter protein. Next, we developed a methodology for recovering an isocline (i.e., a knockout mammalian cell) from a single droplet and transferred it into a standard 96-well plate. Compared to automated systems used for sorting out isoclines in the gene editing pipeline, such as FACS, limited dilution, and clone picking, our system can work with low sample volumes (<200  $\mu\text{L}$ ) and extremely low subpopulation levels (i.e., hard-to-transfect cell lines). The procedure is rapid ( $\approx 45$  min), and gentle on the cells, as our viability and expansion results show. We believe this could be of particular interest for use with other types of cells such as primary or stem cells.

Moving forward, improving alignment, increasing the number of traps, enhancing automation capabilities will greatly improve the functionality of the device. To further increase the throughput of the system, we recommend the integration of image recognition algorithms with our Python based control system and/or improving the automation of the cell recovery process by combining our single-cell isocline technique with other automated droplet recovery techniques.<sup>[95,97]</sup> Taken together, we can envision this multi-functional platform to be used for delivering reagents to isoclines on device, deterministic merging of two populations of single-cell containing droplets, non-binary single-cell sorting, expansion of isoclonal cultures based on their production of extracellular compounds and many other applications. Hybrid microfluidics creates a new pathway for many new mammalian cell assays that have been previously difficult to translate on other types of microfluidic platforms.

### 4. Experimental Section

**Reagents and Materials:** Fabrication materials for hybrid microfluidic devices include a transparent photomask (CAD/Art Services Inc., Bandon, OR), S1811 positive photoresist coated glass slides (Telic, Valencia, CA, USA), MF321 developer (Rohm and Haas, Marlborough, MA, USA), CR-4 chromium etchant (OM Group, Cleveland, OH, USA), AZ-300T photoresist stripper (AZ Electronic Materials, Somerville, NJ, USA), <100> Si wafers (Silicon Valley Microelectronics Inc., Santa Clara, CA, USA), and SU-8 5, SU-8 2035, SU-8 developer (Microchem,

Westborough, MA, USA). Polydimethylsiloxane (PDMS) was purchased from Krayden Inc. (Westminster, CO) and chlorotrimethylsilane from Sigma-Aldrich (Oakville, ON, CA). Polylactic acid (PLA) material for 3D printing was purchased from Shop3D (Mississauga, ON, Canada). DI Water had a resistivity of  $15 \text{ M}\Omega \text{ cm}^{-1}$ .

Reagents for device preparation include 3M Novec HFE7500 engineering fluid and the surfactant 3M Novec 1720 (M.G. Chemicals, Burlington, ON, CA), PEG fluoro-surfactant dissolved in HFE7500 (20 g of 5% wt) (Ran Biotechnologies, Beverly, MA, USA), Fluorinert FC-40 (Sigma-Aldrich), Pluronic F-127 (EMD Millipore Corp, Billerica, MA, USA), and Triton X-100 (Sigma-Aldrich). All glass syringes were from Hamilton, Reno, NV, USA. All tubing and fittings were acquired from IDEX Health & Science, LLC, Oak Harbor, WA. Glass capillaries were purchased from World Precision Instruments (FL, USA). 0.22  $\mu\text{m}$  hydrophobic PTFE membrane was purchased from Thomas Scientific (NJ, USA).

All cell culture and preparation reagents were purchased from Thermo Fisher (Mississauga, ON, Canada). The cell culture reagents include DMEM, RPMI-1640, fetal bovine serum (FBS), penicillin/streptomycin and phosphate buffer saline (PBS) ( $\text{Ca}^{2+}/\text{Mg}^{2+}$  free). The cell viability reagents include Fluorescein diacetate (FDA) ( $5 \mu\text{g mL}^{-1}$ ) and Propidium Iodide (PI) stock solutions ( $2 \mu\text{g mL}^{-1}$ ). For transfection, a Neon Transfection kit (Mississauga, ON, Canada) and Lipofectamine 3000 Transfection Reagent, Genomic Cleavage Detection kit were also purchased. EndoFree Plasmid Maxi Kit for plasmid purification was acquired from Qiagen (Toronto, ON, CA).

**Device Fabrication and Assembly:** The photomasks for the hybrid microfluidic devices were designed using AutoCAD 2017, with an electrode design and dielectric layer on a glass slide ( $50 \times 75 \text{ mm}$ ), and a channel design fitting a 4”-Si wafer. Electrode and dielectric layer fabrication followed standard photolithography procedures reported previously.<sup>[45]</sup> Briefly, chromium-coated substrates with S1811 positive were exposed ( $11 \text{ s}$  at  $38\text{--}50 \text{ mW cm}^{-2}$ ), developed in MF-321 developer, etched with CR-4 chromium etchant, and stripped with AZ-300T photoresist stripper. For the dielectric layer, the devices were placed under plasma oxygen (Harrick Plasma PDC-001, Ithaca, NY) for 1 min 30 s, after which they were immediately spin coated with a SU-8 5 layer (10 s, 500 rpm, 30 s 2000 rpm), soft baked, and exposed to a sawtooth patterned mask. After post-bake, substrates were developed in SU-8 5 developer. A final hard bake cycle was performed by ramping up to  $180 \text{ }^\circ\text{C}$  in 15 min, baking at  $180 \text{ }^\circ\text{C}$  for 10 min and gradual cooling to room temperature. For the channel layer, soft-lithography procedure was followed. Si-wafers were placed under plasma oxygen for 1 min 30 s, after which they are immediately spin coated with SU-8 2035 (500 rpm 10 s and 4000 rpm 30 s). The substrate was soft baked ( $55 \text{ }^\circ\text{C}$  1 min,  $75 \text{ }^\circ\text{C}$  1 min,  $95 \text{ }^\circ\text{C}$  5 min) and exposed under a Quintel Q-4000 mask aligner (Neutronix Quintel, Morgan Hill, CA) ( $10 \text{ s}$  at  $38\text{--}50 \text{ mW cm}^{-2}$ ). Substrates were post baked ( $55 \text{ }^\circ\text{C}$  1 min,  $75 \text{ }^\circ\text{C}$  1 min,  $95 \text{ }^\circ\text{C}$  5 min), and developed in SU-8 5 developer for 3 min 30 s upside down, without shaking. We followed a final hard bake cycle ramping up slowly to  $165 \text{ }^\circ\text{C}$  for 10 min and cooling slowly to room temperature. The master mold was treated with chlorotrimethylsilane vapor deposition in a desiccator for 45 min. PDMS (1:10 w/w ratio curing agent to prepolymer), was poured over the mold and left to cure in an oven at  $65 \text{ }^\circ\text{C}$  for 3 h. Inlets and outlets were made using 0.75 or 0.35 mm biopsy punchers (World Precision Instruments, FL, USA), fitting 1/32” OD tubing or 360  $\mu\text{m}$  OD tubing respectively, after which the PDMS was carefully washed with IPA, DI water, and cleaned with tape to remove debris before device assembly. The PDMS slabs were treated with oxygen plasma for 30 s and directly aligned with the dielectric coated electrodes under a dissecting fluorescence microscope (Olympus IX73, 10X). Device channels were immediately treated with Novec 1720 fluorosilane polymer surfactant for 20 min, under a weight of 750 g. Devices were then air dried (20 min) and baked ( $150 \text{ }^\circ\text{C}$ , 30 min). To connect the droplet generator and the serpentine trap part of the device, a 2 cm piece of PEEK tubing (360  $\mu\text{m}$  OD) was cut and treated with similar Novec 1720 treatment. Outlet blockers were made by hot gluing one end of a 1” PEEK 1/32” OD tubing.

**Device Operation (Trapping, Encapsulation, and Release):** Gastight 500  $\mu\text{L}$  glass syringes were prepared with the fittings and tubing as reported previously, adding one 2.5 mL syringe with a 1.87 mm magnetic stirring disk (V&P Scientific, San Diego, CA, USA). Syringes were installed on a low-pressure neMESYS pump system (Cetoni, Korbussen, DE), installed with a clamp holding a syringe stirrer (Nannostirus, V&P scientific, San Diego, CA, USA). The microfluidics device was placed inside a 3D printed pogo pin holder of which the base plate fits on the stage of an inverted microscope. The flow inside the microfluidic channel was observed under a 4 $\times$  or 10 $\times$  objective under bright-field illumination. Fluid flow and electrode actuation were controlled using an in-house automation system and graphical user interface. In experiments that consisted of trapping, encapsulation, keeping and releasing, we followed a five-step procedure (see Note S3, Supporting Information for automation GUI control). Before priming, a high flow rate ( $\approx 500\text{ nL s}^{-1}$ ) was initiated to avoid air bubbles within the inlets. Priming was performed at a flow rate of 0.8 to 8  $\text{nL s}^{-1}$  with PBS ( $\text{Ca}^{2+}/\text{Mg}^{2+}$  free) containing 2% Pluronic F-127 for 5 min filled in a 500  $\mu\text{L}$  gastight syringe from inlet 1 (I1—see Figure 2). After the device is primed, the flow rate of the priming solution was reduced to 1  $\text{nL s}^{-1}$ . The droplet generator was also flushed with HFE-7500 with 2% fluorosurfactant, from I4. Second, cells re-suspended in  $\text{Ca}^{2+}/\text{Mg}^{2+}$  free-PBS (or in complete media) was placed in a 2.5 mL syringe with a 7 mm magnetic stirring disk. The solution with cells were stirred continuously in the syringe throughout the procedure. The cells were loaded from I1 at a flow rate of 1  $\text{nL s}^{-1}$ , in  $\text{Ca}^{2+}/\text{Mg}^{2+}$  free-PBS or in complete media. Once cells were inside the channel, the priming solution was turned off. MCF-7 cells were used as a model cell line and all reagents prior to operation were filtered sterilized. To trap cells, the filtered MCF-7 cells were resuspended in PBS ( $\text{Ca}^{2+}$   $\text{Mg}^{2+}$  free) and pipetted into a UV sterilized 2.5 mL glass gastight syringe with stirring disk in a laminar hood. Third, droplets were generated by flowing HFE7500 with 2% w/v fluoro-surfactant from I4 at varying flow rates and PBS or media were flowed into the serpentine channel at 0.6  $\text{nL s}^{-1}$  from I3. On-demand droplet generation was performed by actuating electrodes at 15 kHz and 126  $V_{\text{RMS}}$ . Fourth, single-cell encapsulation were performed by connecting tubing from O3 to I2 to encapsulate the trapped cell with a droplet. Phase change for encapsulation was performed using HFE 7500 with 2% w/v fluorosurfactant at a flow rate of 4  $\text{nL s}^{-1}$ . Finally, for forward flow operations (e.g., droplet releasing, keeping or merging), the user used pre-programmed electrode actuation sequences (Figure S5, Supporting Information). To reverse the flow, the tubing in I1 and O1 were removed, and a second oil syringe was connected to O2.

**Cell Culture:** MCF-7 cells were grown and maintained in DMEM containing 10% fetal bovine serum (FBS) with no antibiotics in an incubator at 37  $^{\circ}\text{C}$  with 5%  $\text{CO}_2$ . Human lung squamous cell carcinoma dual-labeled (eGFP, Luciferase) stable NCI-H1299 cells (SCL-C01-HLG; Genecopoeia, Inc, Rockville, MD) were grown in RPMI-1640 containing 10% FBS without antibiotics at 37  $^{\circ}\text{C}$  with 5%  $\text{CO}_2$ . For assays on device, cells were washed with PBS, trypsinized and resuspended in complete growth media. The cells were then centrifuged at 200 rcf for 4 min and the cell pellet was resuspended in either PBS or complete media without FBS to obtain an initial cell concentration of approximately  $2 \times 10^6$  cells  $\text{mL}^{-1}$ . Cells were filtered through a 40  $\mu\text{m}$  cell strainer (VWR, Mississauga, ON, CA) to remove cell clumps. An aliquot of the cell suspension ( $\approx 250\text{ }\mu\text{L}$ ) was pipetted into a syringe for operation. Conditioned media for cell expansion was made by collecting complete growth media from 1-day old 80% confluent NCI-H1299 cells (RPMI-1640 10% FBS, 1% penicillin/streptomycin) and adding 50% fresh complete growth media filter sterilizing and storing it at  $-80\text{ }^{\circ}\text{C}$  until used.

**Viability Assays:** For viability assays, a 1X FDA/PI solution was prepared with 10  $\mu\text{L}$  PI stock and 2.5  $\mu\text{L}$  FDA stock, kept on ice, and used within 2 h. FDA/PI solution was placed in a 500  $\mu\text{L}$  syringe covered with aluminum foil. After trapping of MCF-7 cells, the two top electrodes under each trap (top left under the trap, top right under the main channel) were actuated for 10 s (15 kHz 126  $V_{\text{RMS}}$ ), after which the ground electrode was actuated for 10 s (15 kHz 126  $V_{\text{RMS}}$ ) followed by activating the two bottom electrodes for 10 s (15 kHz 126  $V_{\text{RMS}}$ ). 1X FDA/PI was then flushed through the device at 1  $\text{nL s}^{-1}$  and the device

was incubated in the dark for 10 min. After incubation, MCF-7 cells were imaged (FDA:  $\lambda_{\text{ex}} = 495\text{ nm}$ ,  $\lambda_{\text{em}} = 520\text{ nm}$ , 300 ms exposure; PI:  $\lambda_{\text{ex}} = 535\text{ nm}$ ,  $\lambda_{\text{em}} = 617\text{ nm}$ , 3 s exposure) under a fluorescent microscope (Olympus IX73 Inverted Microscope; Québec City, Canada) and images were analyzed using ImageJ. This process was repeated for control cells (i.e., non-voltage potentiated cells).

**H1299 Transfection:** pCRISPR\_eGFP\_314, pCRISPR\_RAF1\_94 and pCRISPR/Cas9\_All\_in\_one\_LacZ plasmids (Table S3, Supporting Information) were transformed into DH5 $\alpha$  stocks, grown overnight in LB with ampicillin, and purified (endotoxin free). For forward lipid transfection of NCI-H1299 cells with an All-in-one pCRISPR/sgRNA plasmid, on day 0, cells were subcultured in a 24-well plate to reach confluency the day after (day 1). On Day 1, cells were transfected using 5  $\mu\text{g}$  DNA per well. After 48 hours (Day 3), cells were harvested or subcultured into a 6-well plate. Confluent cells were trypsinized, centrifuged (200 rcf, 4 min), strained through a 40  $\mu\text{m}$  filter, and resuspended in either PBS or flow cytometry buffer.

**On-Chip Sorting, Clonal Recovery, and Expansion:** For microfluidic sorting and cell recovery, PBS resuspended cells were loaded into a sterile 2.5 mL syringe with stir disk and 1/32"OD PEEK tubing. The device was primed with PBS with 2% F-127, and transfected NCI-H1299 cells were trapped at 4  $\text{nL s}^{-1}$ . Capillary tubes were filled with HFE-7500 2% fluorosurfactant and placed on the outlet of the single-cell trapping device. pCRISPR\_eGFP\_sg314 and pCRISPR\_RAF1\_sg94 transfected cells were sorted by forward releasing mCherry+/eGFP+ cell containing droplets on-demand. A single droplet containing an isoclone was loaded individually into each capillary. The oil flow was reversed to hydrodynamically release the remaining droplets to waste. For expansion, 20  $\mu\text{L}$  conditioned media was placed on a hydrophobic PTFE membrane situated on a custom 3D printed holder at 37  $^{\circ}\text{C}$ . The single capillary containing the recovered droplet was immediately flushed on top of the conditioned media droplet by 10  $\mu\text{L}$  of FC-40 oil. After 1 min incubation, the droplet was recovered in a 96-well plate containing 50  $\mu\text{L}$  conditioned media per well at 37  $^{\circ}\text{C}$ . After 24 h, single adherent clones could be observed based, representing eGFP or RAF1 knockouts. After five days, the expanded cells were maintained by changing the culture media complete growth media. Clones were incubated in a 96-well plate at 5%  $\text{CO}_2$ , 37  $^{\circ}\text{C}$  to allow expansion to 50% confluency.

**Flow Cytometry and Genomic Cleavage Analysis:** To obtain transfection efficiency, transfected and control cells were resuspended in sorting buffer (1X PBS ( $\text{Ca}^{2+}/\text{Mg}^{2+}$  free), 1 mM EDTA, 25 mM HEPES pH 7.0, 1% FBS, sterilized using a 0.2  $\mu\text{m}$  filter), placed on ice, and loaded in a BD FACS Melody (BD Biosciences, San Jose, CA) after 24 h post-transfection. Gating was performed for forward versus side scatter (FSC versus SSC) on control population after which the positive control fluorescence and transfected population were measured (GFP: 488 nm laser, BP 585/40 nm and mCherry: 488 nm, LP 670 nm). To obtain an estimate of knockout efficiency, a genomic cleavage detection assay (GCD) was performed (GeneArt Genomic Cleavage detection kit, Thermo Scientific) following the manufacturer protocol. Briefly, cell genomic DNA was extracted 48 h post-transfection and  $\sim 500$  bp fragments containing gRNA target sites were amplified using PCR and primers, designed using NCBI primer-BLAST (Table S4, Supporting Information) and BLASTed against *Homo sapiens*. The fragments were re-annealed, and a cleavage reaction was performed using the manufacturer provided endonuclease. A 2% lithium acetate borate gel (10 mM lithium acetate, 10 mM boric acid) was used to resolve the cleavage bands in 20 min at 220 V. Parent and cleavage band intensities were compared to calculate the cleavage efficiency. Expected cleavage bands were shown in Table S5, Supporting Information.

**Data Analysis:** Data analysis was performed with R v3.6.2. Data from Figure 3 was fitted with a three-parameter logistic regression model with continuous predictors (Hosmer-Lemeshow goodness of fit test  $p > 0.05$  for all three models) (Table S6, Supporting Information). Image analysis to calculate droplet volume, and gel analysis were performed using Fiji by ImageJ. Flow cytometry density plots were generated using FlowJo v10. Fluid and electric field simulations were performed with COMSOL 5.4 Multiphysics (Note S2, Supporting Information). All in-house code was written in Python v2.7.15.

## Supporting Information

Supporting Information is available from the Wiley Online Library or from the author.

## Acknowledgements

The authors thank Alisa Piekny's lab for donating MCF-7 cells. They also thank Smita Amarnath and Nicholas Gold for training and helping to run the samples on the flow cytometer in the Genome Foundry affiliated with the Centre of Applied Synthetic Biology (CASB) and for their generous technical support. The authors thank the Natural Sciences and Engineering Research Council (NSERC), the Fonds de Recherche Nature et technologies (FRQNT), and the Canadian Foundation for Innovation (CFI) for funding. K.S. thanks FRQNT B2X and NSERC CREATE SynBioApps program for graduate funding. K.S., F.A., and G.S. thank Concordia University department of Electrical and Computer Engineering for FRS Funding and the Biology Department for academic resources. S.C.C.S. thanks Concordia for a University Research Chair.

## Conflict of Interest

The authors declare no conflict of interest.

## Author Contributions

K.S. built the device, carried out experiments, analyzed the data and wrote custom software. K.S. and S.C.C.S. designed the experiments. F.A. helped in device design, fabrication, and characterization. A.B.V.Q. assisted in cell culture and transfection. G.S. designed automation system software and hardware. K.S. and S.C.C.S. wrote the paper, and all authors reviewed the final version of the manuscript before submission.

## Keywords

digital microfluidics, droplet microfluidics, gene-editing, single-cell, transfection

Received: April 15, 2020

Revised: June 18, 2020

Published online: July 23, 2020

- [1] S. B. Moon, D. Y. Kim, J.-H. Ko, J.-S. Kim, Y.-S. Kim, *Trends Biotechnol.* **2019**, *37*, 870.
- [2] C. A. Vakulskas, D. P. Dever, G. R. Rettig, R. Turk, A. M. Jacobi, M. A. Collingwood, N. M. Bode, M. S. McNeill, S. Yan, J. Camarena, C. M. Lee, S. H. Park, V. Wiebking, R. O. Bak, N. Gomez-Ospina, M. Pavel-Dinu, W. Sun, G. Bao, M. H. Porteus, M. A. Behlke, *Nat. Med.* **2018**, *24*, 1216.
- [3] T. Maruyama, S. K. Dougan, M. C. Truttmann, A. M. Bilate, J. R. Ingram, H. L. Ploegh, *Nat. Biotechnol.* **2015**, *33*, 538.
- [4] X. Dai, J. J. Park, Y. Du, H. R. Kim, G. Wang, Y. Errami, S. Chen, *Nat. Methods* **2019**, *16*, 247.
- [5] X. Liu, Y. Zhang, C. Cheng, A. W. Cheng, X. Zhang, N. Li, C. Xia, X. Wei, X. Liu, H. Wang, *Cell Res.* **2017**, *27*, 154.
- [6] F. J. Sánchez-Rivera, T. Jacks, *Nat. Rev. Cancer* **2015**, *15*, 387.
- [7] T. Zhan, N. Rindtorff, J. Betge, M. P. Ebert, M. Boutros, *Semin. Cancer Biol.* **2019**, *55*, 106.
- [8] A. C. Komor, A. H. Badran, D. R. Liu, *Cell* **2017**, *168*, 20.
- [9] V. T. Chu, T. Weber, B. Wefers, W. Wurst, S. Sander, K. Rajewsky, R. Kühn, *Nat. Biotechnol.* **2015**, *33*, 543.
- [10] A. M. Chakrabarti, T. Henser-Brownhill, J. Monserrat, A. R. Poetsch, N. M. Luscombe, P. Scaffidi, *Mol. Cell* **2019**, *73*, 699.
- [11] F. A. Ran, P. D. Hsu, J. Wright, V. Agarwala, D. A. Scott, F. Zhang, *Nat. Protoc.* **2013**, *8*, 2281.
- [12] R. A. Hughes, A. D. Ellington, *Cold Spring Harbor Perspect. Biol.* **2017**, *9*, a023812.
- [13] A. I. Andreou, N. Nakayama, *PLoS One* **2018**, *13*, e0189892.
- [14] S. J. Moore, H.-E. Lai, R. J. R. Kelwick, S. M. Chee, D. J. Bell, K. M. Polizzi, P. S. Freemont, *ACS Synth. Biol.* **2016**, *5*, 1059.
- [15] M. P. Stewart, A. Sharei, X. Ding, G. Sahay, R. Langer, K. F. Jensen, *Nature* **2016**, *538*, 183.
- [16] H. Yin, K. J. Kauffman, D. G. Anderson, *Nat. Rev. Drug Discovery* **2017**, *16*, 387.
- [17] X. Liang, J. Potter, S. Kumar, Y. Zou, R. Quintanilla, M. Sridharan, J. Carte, W. Chen, N. Roark, S. Ranganathan, N. Ravinder, J. D. Chesnut, *J. Biotechnol.* **2015**, *208*, 44.
- [18] J. J. Priola, N. Calzadilla, M. Baumann, N. Borth, C. G. Tate, M. J. Betenbaugh, *Biotechnol. J.* **2016**, *11*, 853.
- [19] D. Kuystermans, M. Al-Rubeai, in *Animal Cell Culture* (Ed: M. Al-Rubeai), Springer International Publishing, Cham **2015**, pp. 327–372.
- [20] K. Lindgren, A. Salmén, M. Lundgren, L. Bylund, Å. Ebler, E. Fäldt, L. Sörvik, C. Fenge, U. Skoging-Nyberg, *Cytotechnology* **2009**, *59*, 1.
- [21] K. Evans, T. Albanetti, R. Venkat, R. Schoner, J. Savery, G. Miro-Quesada, B. Rajan, C. Groves, *Biotechnol. Prog.* **2015**, *31*, 1172.
- [22] D. Bardin, M. R. Kendall, P. A. Dayton, A. P. Lee, *Biomicrofluidics* **2013**, *7*, 034112.
- [23] J. J. Agresti, E. Antipov, A. R. Abate, K. Ahn, A. C. Rowat, J.-C. Baret, M. Marquez, A. M. Klibanov, A. D. Griffiths, D. A. Weitz, *Proc. Natl. Acad. Sci. USA* **2010**, *107*, 4004.
- [24] M. He, J. S. Edgar, G. D. M. Jeffries, R. M. Lorenz, J. P. Shelby, D. T. Chiu, *Anal. Chem.* **2005**, *77*, 1539.
- [25] M. Navi, N. Abbasi, M. Jeyhani, V. Gnyawali, S. S. H. Tsai, *Lab Chip* **2018**, *18*, 3361.
- [26] I. Barbulovic-Nad, S. H. Au, A. R. Wheeler, *Lab Chip* **2010**, *10*, 1536.
- [27] H. Sinha, A. B. V. Quach, P. Q. N. Vo, S. C. C. Shih, *Lab Chip* **2018**, *18*, 2300.
- [28] J. Li, B. Wang, B. M. Juba, M. Vazquez, S. W. Kortum, B. S. Pierce, M. Pacheco, L. Roberts, J. W. Strohbach, L. H. Jones, E. Hett, A. Thorarensen, J.-B. Telliez, A. Sharei, M. Bunnage, J. B. Gilbert, *ACS Chem. Biol.* **2017**, *12*, 2970.
- [29] A. Sharei, J. Zoldan, A. Adamo, W. Y. Sim, N. Cho, E. Jackson, S. Mao, S. Schneider, M.-J. Han, A. Lytton-Jean, P. A. Basto, S. Jhunjunwala, J. Lee, D. A. Heller, J. W. Kang, G. C. Hartoularos, K.-S. Kim, D. G. Anderson, R. Langer, K. F. Jensen, *Proc. Natl. Acad. Sci. USA* **2013**, *110*, 2082.
- [30] A. Sharei, R. Trifonova, S. Jhunjunwala, G. C. Hartoularos, A. T. Eyerman, A. Lytton-Jean, M. Angin, S. Sharma, R. Pocevicute, S. Mao, M. Heimann, S. Liu, T. Talkar, O. F. Khan, M. Addo, U. H. von Andrian, D. G. Anderson, R. Langer, J. Lieberman, K. F. Jensen, *PLoS One* **2015**, *10*, e0118803.
- [31] T. DiTommaso, J. M. Cole, L. Cassereau, J. A. Buggé, J. L. S. Hanson, D. T. Bridgen, B. D. Stokes, S. M. Loughhead, B. A. Beutel, J. B. Gilbert, K. Nussbaum, A. Sorrentino, J. Toggweiler, T. Schmidt, G. Gyulveszi, H. Bernstein, A. Sharei, *Proc. Natl. Acad. Sci. USA* **2018**, *115*, E10907.
- [32] G. L. Szeto, D. Van Egeren, H. Worku, A. Sharei, B. Alejandro, C. Park, K. Frew, M. Brefo, S. Mao, M. Heimann, R. Langer, K. Jensen, D. J. Irvine, *Sci. Rep.* **2015**, *5*, 10276.
- [33] X. Ding, M. P. Stewart, A. Sharei, J. C. Weaver, R. S. Langer, K. F. Jensen, *Nat. Biomed. Eng.* **2017**, *1*, 0039.

- [34] P. Agrawal, N. P. Ingle, W. S. Boyle, E. Ward, J. Tolar, K. D. Dorfman, T. M. Reineke, *ACS Appl. Mater. Interfaces* **2016**, *8*, 8870.
- [35] F. Chen, Y. Zhan, T. Geng, H. Lian, P. Xu, C. Lu, *Anal. Chem.* **2011**, *83*, 8816.
- [36] X. Li, M. Aghaamoo, S. Liu, D.-H. Lee, A. P. Lee, *Small* **2018**, *14*, 1802055.
- [37] A. Mocciano, T. L. Roth, H. M. Bennett, M. Soumillon, A. Shah, J. Hiatt, K. Chapman, A. Marson, G. Lavieue, *Commun. Biol.* **2018**, *1*, 41.
- [38] F. Lan, B. Demaree, N. Ahmed, A. R. Abate, *Nat. Biotechnol.* **2017**, *35*, 640.
- [39] E. Z. Macosko, A. Basu, R. Satija, J. Nemes, K. Shekhar, M. Goldman, I. Tirosh, A. R. Bialas, N. Kamitaki, E. M. Martersteck, J. J. Trombetta, D. A. Weitz, J. R. Sanes, A. K. Shalek, A. Regev, S. A. McCarroll, *Cell* **2015**, *161*, 1202.
- [40] P. Shahi, S. C. Kim, J. R. Haliburton, Z. J. Gartner, A. R. Abate, *Sci. Rep.* **2017**, *7*, 44447.
- [41] F. Gielen, R. Hours, S. Emond, M. Fischlechner, U. Schell, F. Hollfelder, *Proc. Natl. Acad. Sci. USA* **2016**, *113*, E7383.
- [42] E. Moazami, J. M. Perry, G. Soffer, M. C. Husser, S. C. C. Shih, *Anal. Chem.* **2019**, *91*, 5159.
- [43] M. C. Husser, P. Q. N. Vo, H. Sinha, F. Ahmadi, S. C. C. Shih, *ACS Synth. Biol.* **2018**, *7*, 933.
- [44] L. M. Y. Leclerc, G. Soffer, D. H. Kwan, S. C. C. Shih, *Biomicrofluidics* **2019**, *13*, 034106.
- [45] F. Ahmadi, K. Samlali, P. Q. N. Vo, S. C. C. Shih, *Lab Chip* **2019**, *19*, 524.
- [46] H. Babahosseini, T. Misteli, D. L. DeVoe, *Lab Chip* **2019**, *19*, 493.
- [47] S. Lee, H. Kim, D.-J. Won, J. Lee, J. Kim, *Microfluid. Nanofluid.* **2016**, *20*, 1.
- [48] X. Niu, F. Gielen, A. J. deMello, J. B. Edel, *Anal. Chem.* **2009**, *81*, 7321.
- [49] S. C. C. Shih, G. Goyal, P. W. Kim, N. Koutsoubelis, J. D. Keasling, P. D. Adams, N. J. Hillson, A. K. Singh, *ACS Synth. Biol.* **2015**, *4*, 1151.
- [50] M. W. L. Watson, M. J. Jebrail, A. R. Wheeler, *Anal. Chem.* **2010**, *82*, 6680.
- [51] R. de Ruiter, A. M. Pit, V. M. de Oliveira, M. H. G. Duits, D. van den Ende, F. Mugele, *Lab Chip* **2014**, *14*, 883.
- [52] M. Sauzade, E. Brouzes, *Lab Chip* **2017**, *17*, 2186.
- [53] J.-P. Frimat, M. Becker, Y.-Y. Chiang, U. Marggraf, D. Janasek, J. G. Hengstler, J. Franzke, J. West, *Lab Chip* **2011**, *11*, 231.
- [54] K. Chung, C. A. Rivet, M. L. Kemp, H. Lu, *Anal. Chem.* **2011**, *83*, 7044.
- [55] W.-H. Tan, S. Takeuchi, *Proc. Natl. Acad. Sci. USA* **2007**, *104*, 1146.
- [56] M. Zimmermann, H. Schmid, P. Hunziker, E. Delamarche, *Lab Chip* **2006**, *7*, 119.
- [57] W. Shi, J. Qin, N. Ye, B. Lin, *Lab Chip* **2008**, *8*, 1432.
- [58] E. Brouzes, M. Medkova, N. Savenelli, D. Marran, M. Twardowski, J. B. Hutchison, J. M. Rothberg, D. R. Link, N. Perrimon, M. L. Samuels, *Proc. Natl. Acad. Sci. USA* **2009**, *106*, 14195.
- [59] P. Q. N. Vo, M. C. Husser, F. Ahmadi, H. Sinha, S. C. C. Shih, *Lab Chip* **2017**, *17*, 3437.
- [60] C. Liberale, G. Cojoc, F. Bragheri, P. Minzioni, G. Perozziello, R. L. Rocca, L. Ferrara, V. Rajamanickam, E. D. Fabrizio, I. Cristiani, *Sci. Rep.* **2013**, *3*, 1258.
- [61] C. Wu, R. Chen, Y. Liu, Z. Yu, Y. Jiang, X. Cheng, *Lab Chip* **2017**, *17*, 4008.
- [62] X. Li, A. P. Lee, in *Methods in Cell Biology* (Eds: D. A. Fletcher, J. Doh, M. Piel), Academic Press, San Diego, CA **2018**, p. 35.
- [63] D. J. Collins, A. Neild, A. deMello, A.-Q. Liu, Y. Ai, *Lab Chip* **2015**, *15*, 3439.
- [64] M. Abdelgawad, P. Park, A. R. Wheeler, *J. Appl. Phys.* **2009**, *105*, 094506.
- [65] R. W. R. L. Gajasinghe, S. U. Senveli, S. Rawal, A. Williams, A. Zheng, R. H. Datar, R. J. Cote, O. Tigli, *J. Micromech. Microeng.* **2014**, *24*, 075010.
- [66] S. W. Lee, S. S. Lee, *Microsyst. Technol.* **2007**, *14*, 205.
- [67] S. Jang, B. Lee, H.-H. Jeong, S. Hyung Jin, S. Jang, S. Gyeong Kim, G. Yeol Jung, C.-S. Lee, *Lab Chip* **2016**, *16*, 1909.
- [68] K. Leung, H. Zahn, T. Leaver, K. M. Konwar, N. W. Hanson, A. P. Pagé, C.-C. Lo, P. S. Chain, S. J. Hallam, C. L. Hansen, *Proc. Natl. Acad. Sci. USA* **2012**, *109*, 7665.
- [69] J.-C. Baret, O. J. Miller, V. Taly, M. Ryckelynck, A. El-Harrak, L. Frenz, C. Rick, M. L. Samuels, J. B. Hutchison, J. J. Agresti, D. R. Link, D. A. Weitz, A. D. Griffiths, *Lab Chip* **2009**, *9*, 1850.
- [70] D. J. Collins, T. Alan, K. Helmersson, A. Neild, *Lab Chip* **2013**, *13*, 3225.
- [71] A. M. Nightingale, T. W. Phillips, J. H. Bannock, J. C. de Mello, *Nat. Commun.* **2014**, *5*, 3777.
- [72] A. R. Abate, T. Hung, P. Mary, J. J. Agresti, D. A. Weitz, *Proc. Natl. Acad. Sci. USA* **2010**, *107*, 19163.
- [73] M. J. Jebrail, M. S. Bartsch, K. D. Patel, *Lab Chip* **2012**, *12*, 2452.
- [74] A. Huebner, D. Bratton, G. Whyte, M. Yang, A. J. deMello, C. Abell, F. Hollfelder, *Lab Chip* **2009**, *9*, 692.
- [75] M. A. Khorshidi, P. K. P. Rajeswari, C. Wählby, H. N. Joensson, H. A. Svahn, *Lab Chip* **2014**, *14*, 931.
- [76] A. Dewan, J. Kim, R. H. McLean, S. A. Vanapalli, M. N. Karim, *Biotechnol. Bioeng.* **2012**, *109*, 2987.
- [77] C. Dong, T. Chen, J. Gao, Y. Jia, P.-I. Mak, M.-I. Vai, R. P. Martins, *Microfluid. Nanofluid.* **2015**, *18*, 673.
- [78] J. Melai, C. Salm, S. Smits, J. Visschers, J. Schmitz, *J. Micromech. Microeng.* **2009**, *19*, 065012.
- [79] V. Kumar, N. N. Sharma, *J. Nanotech.* **2012**, *2012*, 312784.
- [80] S. H. Au, R. Fobel, S. P. Desai, J. Voldman, A. R. Wheeler, *Integr. Biol.* **2013**, *5*, 1014.
- [81] P. Zhu, L. Wang, *Lab Chip* **2016**, *17*, 34.
- [82] C. Chang, J. Sustarich, R. Bharadwaj, A. Chandrasekaran, P. D. Adams, A. K. Singh, *Lab Chip* **2013**, *13*, 1817.
- [83] M. T. Chung, D. Núñez, D. Cai, K. Kurabayashi, *Lab Chip* **2017**, *17*, 3664.
- [84] L. M. Fidalgo, C. Abell, W. T. S. Huck, *Lab Chip* **2007**, *7*, 984.
- [85] M. Sesen, T. Alan, A. Neild, *Lab Chip* **2014**, *14*, 3325.
- [86] F. Lan, J. R. Haliburton, A. Yuan, A. R. Abate, *Nat. Commun.* **2016**, *7*, 11784.
- [87] W. Wang, C. Yang, C. M. Li, *Lab Chip* **2009**, *9*, 1504.
- [88] N. Shembekar, H. Hu, D. Eustace, C. A. Merten, *Cell Rep.* **2018**, *22*, 2206.
- [89] J. Clausell-Tormos, D. Lieber, J.-C. Baret, A. El-Harrak, O. J. Miller, L. Frenz, J. Blouwolf, K. J. Humphry, S. Köster, H. Duan, C. Holtze, D. A. Weitz, A. D. Griffiths, C. A. Merten, *Chem. Biol.* **2008**, *15*, 427.
- [90] A. Spiegel, M. Bachmann, G. Jurado Jiménez, M. Sarov, *Methods* **2019**, *164–165*, 49.
- [91] A. Fatima, J. Schuster, T. Akram, M. Sobol, J. Hoeber, N. Dahl, *Stem Cell Res.* **2020**, *44*, 101758.
- [92] L. Mazutis, J. Gilbert, W. L. Ung, D. A. Weitz, A. D. Griffiths, J. A. Heyman, *Nat. Protoc.* **2013**, *8*, 870.
- [93] K. Nakamura, R. Iizuka, S. Nishi, T. Yoshida, Y. Hatada, Y. Takaki, A. Iguchi, D. H. Yoon, T. Sekiguchi, S. Shoji, T. Funatsu, *Sci. Rep.* **2016**, *6*, 22259.
- [94] Q. Zhang, T. Wang, Q. Zhou, P. Zhang, Y. Gong, H. Gou, J. Xu, B. Ma, *Sci. Rep.* **2017**, *7*, 41192.
- [95] R. H. Cole, S.-Y. Tang, C. A. Siltanen, P. Shahi, J. Q. Zhang, S. Poust, Z. J. Gartner, A. R. Abate, *Proc. Natl. Acad. Sci. USA* **2017**, *114*, 8728.
- [96] J. Schoendube, D. Wright, R. Zengerle, P. Koltay, *Biomicrofluidics* **2015**, *9*, 014117.
- [97] K. Langer, H. N. Joensson, *SLAS Technol.* **2019**, *25*, 111.